ISSN 0036-0236, Russian Journal of Inorganic Chemistry, 2021, Vol. 66, No. 10, pp. 1583–1591. © Pleiades Publishing, Ltd., 2021.

INORGANIC MATERIALS AND NANOMATERIALS

Single-Step Hydrothermal Synthesis of Zinc Oxide Micro/Nanostructures

V. Nulu[a] and K. Y. Sohn[a, *]

[a] *Department of Nanoscience and Engineering, Center for Nano Manufacturing, Inje University, 197 Inje-ro, Gimhae, Gyeongnam-do, 50834 Korea*

**e-mail: ksohn@inje.ac.kr*

Received December 12, 2020; revised May 19, 2021; accepted May 27, 2021

Abstract– Herein, we report the single-step synthesis of ZnO nanostructures by a simple urea hydrolysis method. Pure phase ZnO and hydrozincite ($Zn_5(CO_3)_2(OH)_6$) nanostructures are easily obtained separately at the optimized hydrothermal conditions, which involve controlling the urea concentration and reaction parameters such as temperature and time. Outside of these conditions, hydrozincite ($Zn_5(CO_3)_2(OH)_6$) with a small admixture of basic zinc carbonate $Zn_4CO_3(OH)_6 \cdot H_2O$ are obtained as by products. X-ray diffraction and electron microscopy reveal that the obtained ZnO sample is comprised of spherical nanoparticles and have a hexagonal wurtzite crystalline structure. Further, a single-step synthesis approach was developed that produces micron sized rod-shaped ZnO structures.

Keywords: hydrothermal method, urea hydrolysis, ZnO micro/nanostructures

DOI: 10.1134/S0036023621100132

INTRODUCTION

Zinc oxide is a crucial semiconductor material that has been the subject of intense research interest because of its unique properties and versatile applications. Nanoparticle ZnO has received particular attention because it is a wurtzite-type semiconductor with a direct bandgap energy of 3.37 eV at room temperature, and a considerable excitation binding energy of about 60 meV, which is significantly larger than other metal oxides [1–4]. Zinc oxide has a unique combination of physical, chemical, biological, electrical, and optical properties, environmental stability, low cost, and easy availability; thus, it finds applications in a wide range of fields such as gas sensors, catalysis, resonators, field-effect transistors, short-wave optics, transparent electronics, ultraviolet (UV) light emitters, piezoelectric devices, and spin electronics [1–7]. The US Food and Drug Administration (FDA) have certified ZnO nanoparticles as being safe for use in FDA-regulated products [8, 9]. Therefore, the synthesis of fine ZnO particles is of great importance. Recently, various techniques have been adopted to synthesize ZnO nanostructures, including physical, chemical, and biological methods such as spray pyrolysis, thermal decomposition, physical or chemical vapor deposition, sol-gel, hydrothermal, co-precipitation, solvothermal methods and synthesis by using plant extracts [10–16]. These methods usually require highly sophisticated equipment, multiple synthesis steps, and high temperatures. Alternatively, low-temperature chemical methods such as co-precipitation, hydrothermal, and hydrolysis methods are cost-effective, easy to handle, and scalable [13].

Several previous studies have fabricated ZnO with different nanostructures by the hydrothermal method. The precipitation of Zn^{2+} ions in the presence of decomposing urea at 90°C was investigated, where the parameters pH and heating time had a significant effect on the colloidal behavior of the particles [17]. For producing ZnO-based varistors, a urea process was used in which $Zn(NO_3)_2$ and other metal nitrates solution was denitrated with urea at reaction temperatures of up to 250°C in a closed reactor, and then the solid residue was additionally calcined at 675°C [18]. Uniform particles of basic zinc carbonate were precipitated from the solution with decomposing urea at 90°C from the $ZnSO_4$, $ZnCl_2$, and $Zn(NO_3)_2$ solution; then the obtained precipitate was subsequently calcined to produce ZnO nanostructures [19, 20]. Music et al. investigated the urea decomposition process to synthesize ZnO, in which zinc carbonate initially was obtained as a final product, and then ZnO phase was produced by heating at ≥300°C [21]. In another study, ZnO did not crystallize upon hydrothermal treatment of 0.2 M $Zn(NO_3)_2$ aqueous solutions containing 1.0 M urea up to 160°C; instead, a hydrozincite phase was formed. ZnO powder was then produced by thermal treatment of the hydrozincite in the air [22]. Further, ZnO 1D nanostructures have received considerable interest for more than a decade due to their excel-

lent electronic, optical, and life science applications [23, 24]. By reducing size, the mechanical, electrical, chemical, and optical properties are drastically enhanced. Also, in comparison with 0D and 2D nanomaterials, 1D structural features offer ideal electrical transport process and suitable model system to study the electrical and optoelectronic properties on the size reduction and dimensionality [24]. Wang et al., reported that 1D structures of ZnO increase photoconductivity and electron mobility [25]. A similar other report stated that 1D nanostructures significantly increase the active contact surface area and thus improving electrical mobility and device performance [26]. All these approaches dealt with multi-step processes and could not easily produce high yields. From the survey of the literature, it is observed that limited attempts have been made to obtain ZnO nanoparticles/ micro 1D structures using one-step chemical methods. The major motive behind developing such a one-step chemical method is the minimization of the multiple synthesis stages that marks material loss, avoid further heat treatment that outbreak phase purity and grain boundaries of nano ZnO by the aggregation of particles. Also, evade the addition of surfactants that need extra steps to remove from final product. The most important advantage of our approach in comparison with other important studies is the single-step nature of the chemical synthesis without the utilization of further heat treatment, using organic templates, and yielding gram-scale quantities. Recently, devices based on 1D and nanoparticles of ZnO are consistently being developed, such as light-emitting diodes, sensors, photodetectors and transistors. Because these devices performing better than the devices fabricated from thin films and bulk particles. Due to the adverse environmental and health effects of ultrafine nanostructures (<5 nm), instead the usage of nano or micron-sized particles (>10 nm) are advisable for practical device applications. Thus, it is desirable to develop nano/microstructures of ZnO by an environmentally friendly one-step synthesis process to achieve scalable low-cost mass production.

In the present study, we have synthesized ZnO micron-sized structures using a typical two-step urea-assisted hydrothermal method. Importantly, a single-step synthesis process was developed to produce ZnO nanoparticles, without the use of any template or annealing treatment. In addition, we found that slightly varying the reaction parameters in this method would result in scalable ZnO 1D micro- or nanostructures.

EXPERIMENTAL

Materials. Zinc nitrate ($Zn(NO_3)_2{\cdot}6H_2O$) and urea (NH_2CONH_2) were procured from Sigma-Aldrich Limited. All the reagents were of analytical grade and used without further purification.

Preparation of ZnO nanoparticles by urea hydrolysis method. For the synthesis, we have adopted the urea-assisted hydrothermal method. Four experiments were conducted to optimize the ZnO nanoparticle preparation conditions. Initially, four experiments were conducted with constant $Zn(NO_3)_2 \cdot 6H_2O$ concentration of 0.05 M, while the amount of urea (NH_2CONH_2) was varied (0.1 M, 0.05 M, and 0.03 M) at 180°C, and the operating temperature was reduced to 160°C for the fourth experiment. For the first three experiments, the chemicals were dissolved in 400 mL of double-distilled water; then, the solution was transferred to a stainless-steel autoclave with 700 mL capacity. The autoclave was programmed to reach 180°C in 1 h (ramp time), and the reaction was kept for 2 h (soak time) with a stirring speed of 400 rpm. During the experiment, an in-situ pressure of around 18–19 kg cm^{-2} was developed. For the fourth experiment, the temperature was reduced to 160°C for 1 h while maintaining all other parameters as above. To compare the amount of urea effect on the ZnO phase formation, we experimented with 0.04 M urea concentration while the other experimental conditions were the same as that maintained for the initial three experiments. After the autoclave was cooled to room temperature, the precipitates were washed with double distilled water using a Hermle Labortechnik (Type: 2383) ultra-speed centrifuge (maximum 10.000 rpm). The washed precipitates were dried at room temperature and denoted as Z1, Z2, Z3, Z4 and Z5 respectively, as in Table 1. After the first step, the separated precipitates of samples Z1, Z2, and Z4 were subjected to heating at 300°C for 30 min in the air to obtain the ZnO phase; these annealed samples were denoted as Z1C, Z2C, and Z4C respectively. To check the reproducibility for the final product two samples were prepared by following the same experimental conditions as Z3 and the results are reported in table 1 with samples coded as Z3-1 and Z3-2. For preparation of ZnO rod-shaped structures, after the completion of the third experiment with 0.03 M of added urea (Z3), the stirring condition was stopped, and the reaction mixture was kept soaking for 10 h under similar experimental conditions, then the precipitate was separated by centrifugation and dried at room temperature, denoted as Z3r.

Characterization. The phase and composition of the synthesized samples were characterized by powder X-ray diffraction (Siemens D5000 XRD), using CuK_α radiation (1.5406 Å). The morphologies of the as-prepared samples were analyzed using scanning electron microscopy (SEM; Hitachi S520) and transmission electron microscopy (TEM; Phillips Tecnai G2 FEI F12). UV–Vis absorption spectra of the samples, in the form of KBr pellets, were recorded on a Cintra UV-Vis spectrophotometer at wavelengths from 250 nm to 800 nm. Fourier transform infrared spectra (FTIR) were recorded at room temperature using a Perkin-Elmer spectrometer (Model 2000). The specimens

Table 1. Experimental conditions for the preparation of samples from an aqueous solution of $Zn(NO_3)_2 \cdot 6H_2O$ with decomposing urea

Sample	$Zn(NO_3)_2 \cdot 6H_2O$ (M)	Urea, M	Temperature, °C	Reaction Time, h	XRD (as prepared); Final product (g)	Yield, %	XRD (after calcination)
Z1	0.05	0.1	180	3	Hydrozincite; 2.8	–	ZnO (Z1C)
Z2	0.05	0.05	180	3	Hydrozincite; 3.6	–	ZnO (Z2C)
Z3	0.05	0.03	180	3	ZnO; 2.84	48.80	–
Z3-1	0.05	0.03	180	3	ZnO; 2.62	45.05	–
Z3-2	0.05	0.03	180	3	ZnO; 2.71	46.54	–
Z4	0.05	0.03	160	3	Hydrozincite; 3.54	–	ZnO (Z4C)
Z5	0.05	0.04	180	3	ZnO with minor Hydrozincite phase 3.2	–	–

were pressed into small discs using a spectroscopically pure KBr matrix with a pure KBr pellet as the reference. Room temperature photoluminescence (RTPL) was recorded with a Flurolog-3 fluorescence spectrophotometer (Horbia Jobin Yvon) using a Xe lamp as the excitation source.

RESULTS AND DISCUSSION

The urea concentration, reaction temperature, and reaction time of the samples denoted as Z1, Z2, Z3, Z4 and Z5 are tabulated in Table 1, including the annealed samples and the obtained yields. Figure 1 shows X-ray diffraction patterns of the synthesized powders with different urea concentrations. It can be seen that Z1, Z2, and Z4 patterns match well with the hydrozincite ($Zn_5(CO_3)_2(OH)_6$) phase (JCPDS card No. 72-1100) with small additional peaks of basic zinc carbonate $Zn_4CO_3(OH)_6 \cdot H_2O$ evident. Whereas, spectra related to Z3, Z1C, Z2C, and Z4C demonstrate typical diffraction peaks of highly crystalline ZnO wurtzite structure (JCPDS card No. 5-664). Apart from significant peaks in Z1C spectra, minor uncountable additional peaks of hydrozincite still appear. In contrast, XRD spectra of Z3 present broader and less intense diffraction peaks compared to annealed samples, indicating lower crystallinity and smaller particle size than other samples. The crystallite sizes were determined by Scherrer's method: Z3, Z1C, Z2C, and Z4C had average particle sizes of D = 33(3), 152(4), 99(6), and 96(6) nm, respectively. Whereas, sample Z5 is a combination of ZnO with minor hydrozincite impurity peaks (See Table 1).

Figure 2a shows the SEM image of the as-prepared ZnO (Z3) sample, which appears to be a collection of agglomerated nanoscale particles with an unattached appearance. The agglomerated particles neck with their neighbors, forming elongated spindle-like shapes with intermittent voids, which were helpful to improve the resultant surface area. The SEM images in Figs. 2b–2d shows the particle morphologies of Z4, Z4C, Z2C and the inset of image d shows the surface morphology of Z2 sample. The red colored arrows in Fig. 2c represents porous nature of the obtained aggregated particles. The powders produced have particle sizes that are not well distinguished, and it should be noted that some particles might be crystallite agglomerates, which experienced the onset of sintering during the thermal decomposition of Z4 and Z2. Sample Z1 (Fig. 2e) consists of agglomerates of micron-sized rods ended with hexagonal facet (marked with an arrow), along with some portion of smaller particles with irregular shapes. After heating Z1 at 300°C, the SEM in Fig. 2f shows that it is comprised of bundles of aggregated micron-sized hexahedrons with unevenly shaped rods with a thickness of between 1–5 μm. Figure 2g shows an amalgamation of micron and nano-sized needles of Z3r produced by extending the soaking time of the Z3 reaction mixture at the same hydrothermal conditions for about 10 h and the nano-sized rods were distinguished by the arrows. Figure 2h is the X-ray powder diffraction spectra of the sample Z3r, in which all the diffraction reflections represent ZnO phase; a definite line broadening of the diffraction peaks is an indication that the particles are highly crystalline with large particle size. Pacholski et al. [27] and Penn and Banfield [28–30] have observed a phenomenon where smaller nanostructures such as nanoparticles undergo attachment or coalescence to form larger dimension nanostructures. In this study, we found some NRs (nanorods) of hydrozincite (see Fig. 2e) that are built out of bundling of smaller diameter NRs. We believe thin diameter NRs grow as bundles initially and eventually coalesce to form large-diameter micron-sized rods. The reason for this could be the lowering of surface energy. A similar idea that we considered for the evolution of micro- or nano-sized ZnO rods in the Z3r sample is the coagulation of fine ZnO particles of Z3. Also, in the case of Z3, the fact that all the free Zn^{2+} in the solution has been consumed. However, the fact that as the yield approaches 100% indicates that the free Zn^{2+} ions supply is already running out. There-

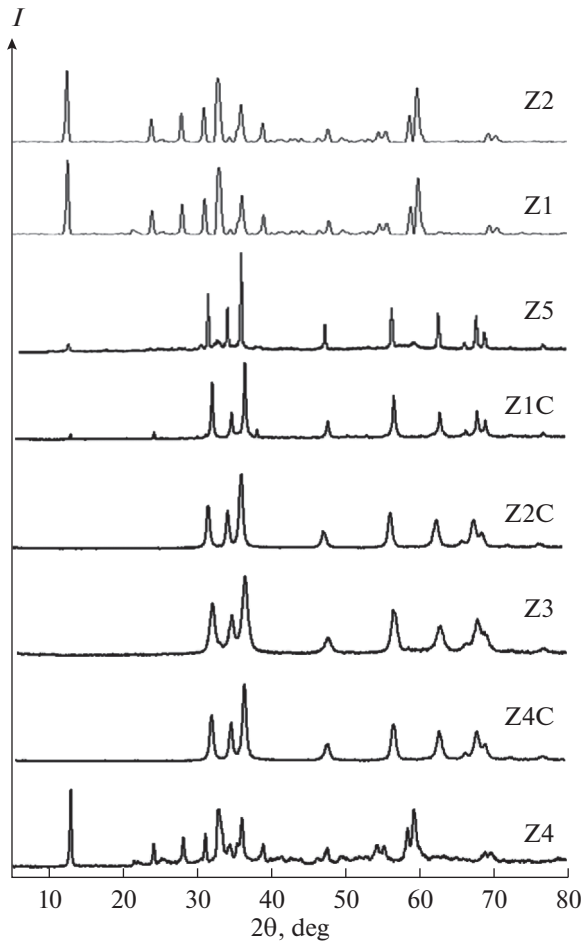

Fig. 1. Characteristic peaks of the X-ray powder diffraction patterns of as-prepared ZnO (Z3), hydrozincite $Zn_4CO_3(OH)_6 \cdot H_2O$ or $Zn_5(OH)_6(CO_3)_2$ (Z4), ZnO with minor hydrozincite impurities (Z5) and thermal decomposition products of samples Z1, Z2, and Z4 at 300°C are depicted. The measurements were made at room temperature.

fore, the continuing increase in length with time could be attributed to a dissolution-precipitation process where small NRs dissolve and larger NRs keep growing until the process reaches equilibrium. An increase in urea concentration from 0.05 to 0.1 M for the Z1 experiment (see Table 1) caused a high amount of in situ generated carbonates that may increase reaction pH to mild basic, and this has resulted in sizeable micron-sized hydrozincite rods. The homogeneity of the micron-sized rods and their shape was preserved after annealing the Z1 sample (i.e., Z1C, see Fig. 2f) with an average diameter of the order of ~1.5 μm.

TEM observation of Z1C and Z2C samples (Figs. 3a, 3b) revealed particles with irregular shapes obtained from the aggregation of nanoparticles. The TEM image of sample Z4 (see Fig. 3c) shows aggregates of hydrozincite particles of irregular shape, and that of sample Z4C (see Fig. 3d) shows that annealing treatment encourages the aggregation of small particles into irregular shapes with larger particle sizes. Figures 3e, 3f exhibit a substantially higher concentration of as-prepared ZnO hexahedrons (Z3) in combination with spherical particles, which showed the tendency to form chain-like structures interconnected with each other. The as-prepared ZnO powder has a homogeneous morphology of nanosized particles with size from 30 to 40 nm. Cheon et al. reported that there are four different parameters such as kinetic energy barrier, temperature, time, and capping molecules that can influence the growth pattern of nanocrystals under non-equilibrium dynamic growth conditions in the solution-based approach [31–34]. In our synthesis process, the temperature, pH value of solution after the reaction, and reaction time are playing a pivotal role. The hydrothermal process without an organic template with the reduced urea content used for Z3 sample synthesis was responsible for a decrease in the final pH of reaction to 6.20; this mild acidic environment potentially restricted particle aggregation and thus causing the formation of fine ZnO particles (Figs. 3e, 3f).

Furthermore, the growth rate of particles along the *c* axis increased with increased reaction time at our hydrothermal conditions. Consequently, ZnO rods with inhomogeneous shape and size are obtained (Fig. 2g), and further studies are needed to improve the uniformity and yield of ZnO nano- and micro-rods. FTIR studies were used to compare the surface purity of the ZnO nanoparticles (Z3) the hydrozincite sample (Z4). The FTIR spectra of samples Z3 and Z4 are shown in Fig. 4a (curves *1*, *2*). Figure 4a (curve *1*) shows the FTIR spectra of sample Z3, with IR bands at 520, 460 and a weak shoulder at 440 cm^{-1} that can be assigned to phase pure ZnO [35–38]. Besides, a split at 440 to 520 cm^{-1} indicates the presence of a combination of well-crystallized particles, is in agreement with the SEM and TEM results. The main features of the IR spectrum of Z4 (Fig. 4a (curve *2*)) correspond to basic zinc carbonate. This spectrum indicates the presence of carbonate groups by a split ν_3 frequency with bands at 1505 and 1387 cm^{-1}. Besides, carbonyl group features relating to ν_1 frequency at 1047 cm^{-1}, ν_2 at 830 cm^{-1}, and ν_4 at 708 cm^{-1} were also visible. These IR bands of the carbonate group are well documented in reference literature [32, 33]. The broadband centered at 3391 cm^{-1} can be ascribed to the stretching vibrations of H_2O molecules, and structural OH groups in hydrogen bonding contributed to the observable IR bands centered at 3408 and 3502 cm^{-1} [30].

A comparison of the surface absorption properties of ZnO nanoparticles (Z3) with the calcined sample Z4C is meaningful because both samples were prepared with the same amount of added urea. Figure 4b shows the UV-vis absorption spectra for the selected Z3 and Z4C samples. For both samples, intense absorption in the UV region is observed between 200 to 400 nm. Absorption peaks of Z3 and Z4C occur at

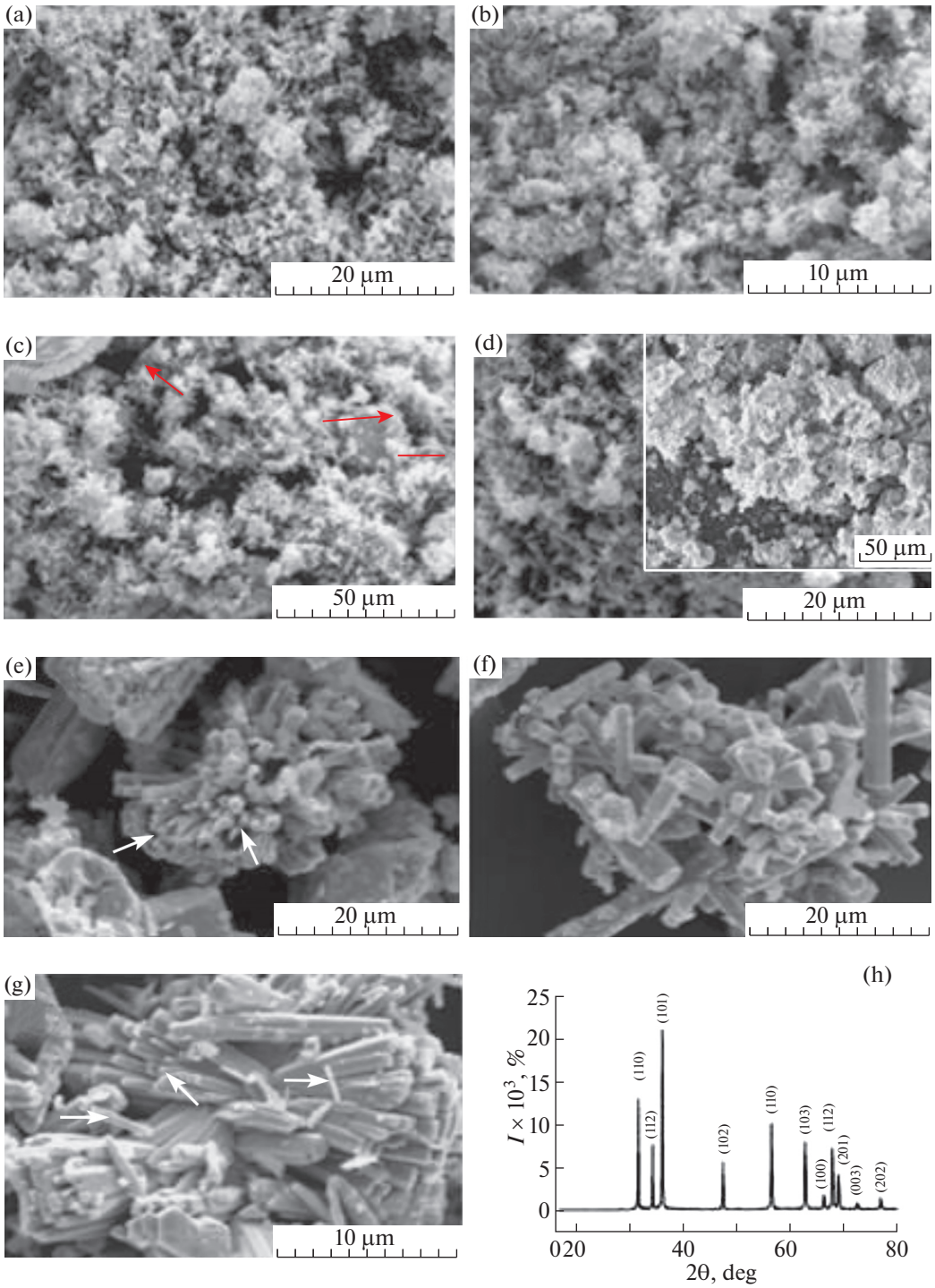

Fig. 2. SEM images of the samples (a) Z3, (b) Z4, (c) Z4C, (d) Z2C inset shows Z2, (e) Z1, (f) Z1C, and (g) SEM image of Z3r and (h) is the X-ray powder diffraction pattern of Z3r sample.

361 and 366 nm, respectively. These peaks are effectively blue-shifted relative to the bulk ZnO absorption at 385 nm owing to the quantum confinement effect, implying smaller nanoparticles [39]. There is a minor absorbance peak was noted above 400 nm (between 450–500 nm) for sample Z4C that could be due to the light-scattering caused by minor remained hydrozincite while with pure ZnO nanoparticles (Z3) that was negligible (see Fig. 4b (curves *1*, *2*)). Band gaps of 3.43 and 3.39 eV were obtained for samples Z3 and calcined Z4C, respectively, that are close to the reported value of 3.37 eV [40].

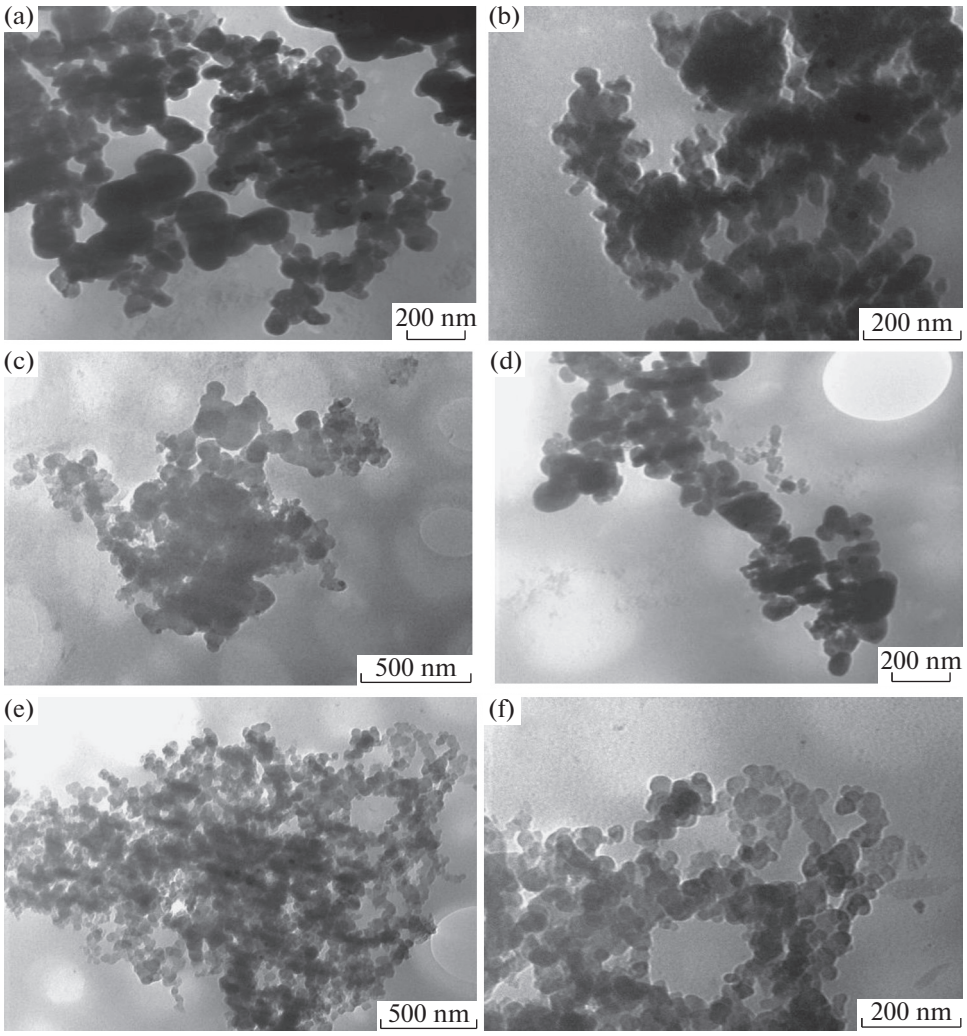

Fig. 3. TEM images of samples (a) Z1C, (b) Z2C, (c) as prepared hydrozincite, Z4, (d) Z4C, and (e, f) Z3 at different magnifications.

It is well known that there are two kinds of emission bands of UV and visible (green or yellow) spectra in ZnO crystals [41, 42]. The emission in the UV region is characteristic of the recombination between electrons in the conduction band and holes in the valence band [43, 44]. The visible emission is related to defects, similarly to deep level emissions, such as oxygen vacancies and Zn interstitials [45, 47]. Therefore, a study of the RTPL properties of ZnO can provide valuable information on the quality and purity of this material, as shown in Fig. 4c (curves *1*, *2*), the obtained products display a strong UV emission at around 395 and 396 nm, respectively. The UV luminescence band is characteristic of the reduced state of ZnO crystals, and the intense UV luminescence can indicate an increased concentration of oxygen vacancies. The well-known stronger and broader emission situated in the yellow-green part of the visible spectrum of Z3 is less intense than Z4, which suggests that the as-obtained ZnO nanoparticles for Z3 are highly pure and crystalline with a rather low-concentration of oxygen vacancies [45, 48]. Comparatively, the intensity of Z4C is enhanced, which is attributed to the annealing treatment causing an increase in crystallite size of ZnO particles and a subsequent decrease in quantum effects.

Typically, in previous studies, ZnO was prepared by urea hydrolysis from the intermediate precipitate zinc carbonate hydroxide hydrate product, and then zinc oxide is crystallized under a forced state, i.e., after calcination. During the reaction, urea decomposes with a rise in temperature of more than 100°C and is expected to provide the following stepwise reactions [45]:

$$CO(NH_2)_2 \rightarrow NH_3 + HNCO \leftrightarrow NH_4^+ + NCO^-. \quad (1)$$

In a strongly acidic medium, the urea decomposition is accelerated due to the rapid quantitative conversion of the cyanate ion.

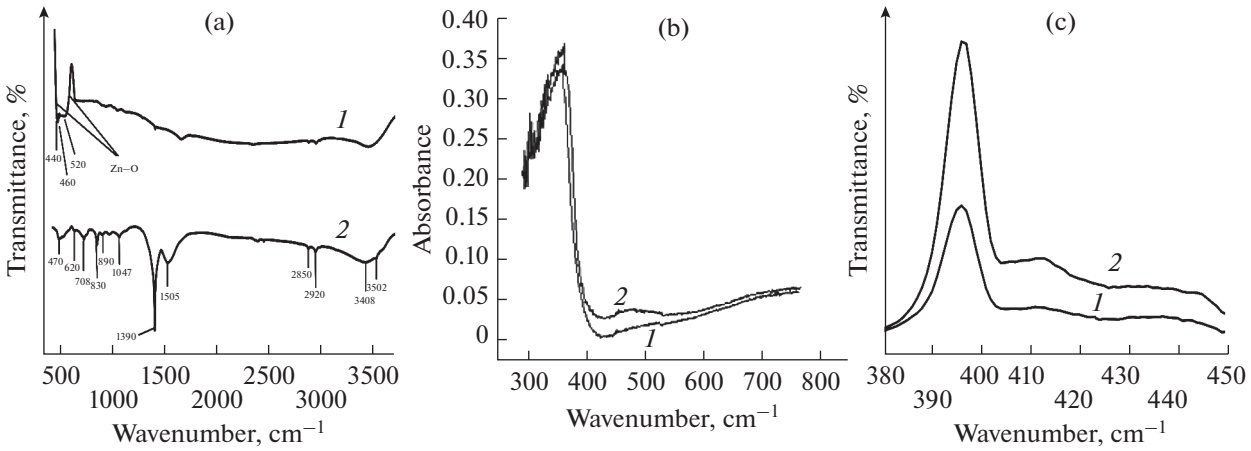

Fig. 4. (a) FTIR spectra, (b) UV-spectrum of samples (*1*) Z3 and (*2*) Z4C; (c) RTPL spectra of samples Z3 (*1*) and Z4C (*2*), respectively. All spectra were recorded at room temperature.

$$NCO^- + 2H^+ + H_2O \rightarrow NH_4^+ + CO_2, \quad (2)$$

while in weak acidic, neutral, and alkaline solutions, the hydrolysis can be represented by

$$NCO^- + OH^- + H_2O \rightarrow NH_3 + CO_3^{2-}. \quad (3)$$

The hydrolyzed product reacts with zinc nitrate to form zinc carbonate hydroxide hydrate:

$$4Zn^{2+} + CO_3^{2-} + 6OH^- + H_2O \rightarrow Zn_4CO_3(OH)_6 \cdot H_2O \downarrow. \quad (4)$$

As per Eq. (1), the NH_4^+ generated was reacted with $(NO_3)^-$ obtained from starting material $Zn(NO_3)_2 \cdot 6H_2O$.

$$xNH_4^+ + xNO_3^- \rightarrow xNH_4NO_3. \quad (5)$$

In the next step, zinc carbonate hydroxide hydrate samples (Z1, Z2 in this work) calcined at 300°C for 30 min would result in zinc oxide:

$$Zn_4CO_3(OH)_6 \cdot H_2O \rightarrow 4ZnO + 4H_2O + CO_2\uparrow. \quad (6)$$

From the tabulated values (Table 1), it is clear that ZnO phase is directly attained by autoclaving 0.03 M of $Zn(NO_3)_2 \cdot 6H_2O$ at the high reaction temperature 180°C (pH 6.1). From our tabulated results, a decrease in temperature from 180 to 160°C for Z4 sample while maintaining other reaction conditions as same as of Z3 would result in the hydrozincite phase. Besides, an increase in urea concentration from 0.03 M to 0.05 (Z2) and 0.1 M (Z1) at 180°C would also produce hydrozincite phase, while by adjusting urea amount to 0.04 M resulted hydrazincite with minor ZnO impurity peaks (sample Z5) which demonstrating that reaction temperature and urea concentration significantly affect the final product phase. Besides, in the above experimental conditions, in-situ generated pressure values during the autoclaving of the reactions are 20 kg cm^{-2} for Z1, 19 kg cm^{-2} for Z2, 19 kg cm^{-2} for Z3, and 11 kg cm^{-2} for Z4, respectively. In the present work, for sample Z4 at 160°C, the urea decomposition is probably progressed according to Eq. (3), and the observed final pH was 6.5. It can be seen that, although we maintained similar experimental conditions for Z3 and Z4 except for a change in temperature, one would expect an increase in temperature significantly increases the in situ generated pressure from 11 kg cm^{-2} to 19 kg cm^{-2} that would affect the nature of the final product. We believe that at this high pressure, together with the low concentration of urea, directly produces pure ZnO powder without any intermediate hydrozincite phase formation. To understand the reason behind this, we referred to similar studies [49–52]. In mild alkaline conditions, the hydrolysis of urea proceeds slowly (see Eq. (3)) and the supply of the OH^- ions is insufficient to promote the dehydration reaction due to the presence of carbonate ions; instead, the carbonate ions in the weak acidic conditions prefer the formation of $Zn_4CO_3(OH)_6 \cdot H_2O$ through heterogeneous nucleation arising from hydroxide condensation under the small degree of supersaturation. The *x* moles of remaining nitrate ions react with *x* moles NH_4^+ ions (possible by product in Eq. (1)) as shown in Eq. (5). For high-pressure and high-temperature experiments, it was reported that the carbonate ion dissolves in aqueous solution by forming a complex with OH^- ions [52]. The equilibrium molar reaction:

$$CO_3^{2-} + H_2O = HCO_3^-OH^-. \quad (7)$$

It entails a decrease in the concentration of carbonate ions with the increase in pressure. Due to this reason, in our Z3 sample preparation experiment, we hypothesized that insufficient free carbonate ions were left in the solution to react with $Zn(NO_3)_2 \cdot 6H_2O$ to form hydrozincite; consequently, hydrolysis of Zn^{2+} ions proceeds by another suitable path with OH^- ions

that possibly exist in weak acidic conditions, which in turn react with Zn^{2+} to form oxide:

$$2OH^- + Zn^{2+} \rightarrow ZnO_{(s)} + H_2O. \quad (8)$$

As reported by Chang et al., weak acidic reaction conditions can feasibly result in the formation of ZnO particles [14]. Besides, as shown in Table 1, our experimental conditions are useful for precipitating ZnO particles in the nanometer range (30–40 nm) shown in Fig. 3d with 69.72% of actual yield for Z3 compared to the theoretical yield. Also, for Z3-1 and Z3-2 samples, the obtained yields are more than 60% those are good and acceptable, however, the decrease in this yield is due to the loss of some product during sample collection from the hydrothermal reactor and while washing treatment. Also, we believe that the low amounts of urea used for Z3, Z3-1 and Z3-2 samples leads to incomplete solid precipitation that which resulted with decreased amount of final product. The reduced in urea amount together with the long soaking time resulted with nanorods, as was supported by reported similar approaches [17, 50] and Vayssieres et al. [53–55] reported the diameters of rods and tubes could be brought into the nanometer range by reducing the concentration of reactants.

CONCLUSIONS

In conclusion, a one-step urea-assisted hydrothermal approach was employed to produce ZnO nanoparticles and micron rods by varying the metal precursor to urea concentration ratio, reaction time, and temperature. It is found that while autoclaving at 0.03 M urea and 180°C reaction temperature, under hydrothermal conditions, the autogenous pressure facilitates the hydrolysis of Zn^{2+} ions with OH^- ions resulting in the formation of ZnO nanoparticles. Furthermore, the direct synthesis of ZnO micro-sized rods was achieved by further aging the reaction mixture in an autoclave without stirring for 10 h. As the concentration of urea was increased, carbonate concentration was proportionally increased, which leads to the formation of hydrozincite phase. The resultant ZnO nanoparticles delivered excellent optical properties that were comparable with similar reported materials. The effect of urea concentration on the ZnO phase and morphology was studied. This synthesis method is highly reproducible, yields gram quantities easy to handle, and industrially applicable. We propose that this method can also be extended for other metal oxides synthesis.

ACKNOWLEDGMENTS

This work was supported by the 2016 Post-doctoral Research Program of Inje University.

CONFLICT OF INTEREST

The authors declare that they have no conflicts of interest.

REFERENCES

1. K. Nomura, H. Ohta, K. Ueda, et al., Science **300**, 1269 (2003). https://doi.org/10.1126/science.1083212
2. D. Li and H.J. Haneda, Chemosphere **51**, 129 (2003). https://doi.org/10.1016/S0045-6535(02)00787-7
3. T. Nakada, Y. Hirabayashi, T. Tokado, et al., Sol. Energy. **77**, 739 (2004). https://doi.org/10.1016/j.solener.2004.08.010
4. M.S. Arnold, P. Avouris, Z.W. Pan, et al., J. Phys. Chem. B **107**, 659 (2002). https://doi.org/10.1021/jp0271054
5. V.A.L. Roy, A.B. DjuriSic, W.K. Chan, et al., Appl. Phys. Lett. **83**, 141 (2003). https://doi.org/10.1063/1.1589184
6. P.X. Gao, Y. Ding and W.L. Wang, Nano Lett. **3**, 1315 (2003). https://doi.org/10.1021/nl034548q
7. S. Y. Lee, E. S. Shim, H. S. Kang, et al., Thin Solid Films **437**, 31 (2005). https://doi.org/10.1016/j.tsf.2004.06.194
8. A. Emamifar, M. Kadivar, and S.S. Zad, Inn. Food Sci. Emerg. Technol. **11**, 742 (2010). https://doi.org/10.1016/j.ifset.2010.06.003
9. J. Sawai, J. Microbiol. Meth. **54**, 177 (2003). https://doi.org/10.1016/S0167-7012(03)00037-X
10. S. Panigrahi, S. Kundu, S. Kumar Ghosh, et al., J. Nanopart. Res. **6**, 411 (2004). https://doi.org/10.1007/s11051-004-6575-2
11. Y. Zhou, W. Wu, G. Hu, et al., Mater. Res. Bull. **43**, 2113 (2008). https://doi.org/10.1016/j.materresbull.2007.09.024
12. J. M. Li, X. L. Zeng, Q. Huang, et al., Cryst. Eng. Comm. **14**, 7800 (2012). https://doi.org/10.1039/C2CE25963J
13. D. Raoufi, Renew. Energy **50**, 932 (2013). https://doi.org/10.1016/j.renene.2012.08.076
14. V. Gerbreders, M. Krasovska, E. Sledevskis, et al., CrystEngComm **22,** 1346 (2020). https://doi.org/10.1039/D0CE00989J
15. B. Liu and H. Chun Zeng, J. Am. Chem. Soc. **15**, 4430 (2003). https://doi.org/10.1021/ja0299452
16. L. N. Dem'yanets, L. E. Li, T. G. Uvarova, et al., Inorg. Mater. **40**, 1173 (2004). https://doi.org/10.1023/B:INMA.0000048217.41184.c8
17. K.G. Kanade, B.B. Kale, R.C. Aiyer, et al., Mater. Res. Bull. **41**, 590 (2006). https://doi.org/10.1016/j.materresbull.2005.09.002
18. E. Sonder, T.C. Quinby and D.L. Kinser, Am. Ceram. Soc. Bull. **65**, 665 (1986). https://doi.org/10.2172/5331308
19. M. Castellano and E. Matijevic, Chem. Mater. **1**, 78 (1989). https://doi.org/10.1021/cm00001a018

20. L.N. Dem'yanets, L.E. Li and T.G. Uvarova. J. Cryst. Growth **287**, 23 (2006). https://doi.org/10.1016/j.jcrysgro.2005.10.036

21. P. Tonto, O. Mekasuwandumrong, S. Phatanasri, et al., Ceram. Int. **34**, 57 (2008). http://dx.doi.org/doi:10.1016/j.ceramint.2006.08.003

22. H. Wang, J. Xie, K. Yan, et al., J. Mater. Sci. Technol. **27**, 153 (2011). https://doi.org/10.1016/S1005-0302(11)60041-8

23. M. Søndergaard, E. D. Bøjesen, M. Christensen, et al., Cryst. Growth Des. **11**, 4027 (2011). https://doi.org/10.1021/cg200596c

24. W. A. Heer, A. Chatelain, and D. Ugarte, Science **270**, 1179 (1995). https://doi.org/10.1126/science.270.5239.1179

25. Z. L. Wang, Mater. Sci. Eng. R **64**, 33 (2009). https://doi.org/10.1016/j.mser.2009.02.001

26. A. A. Chaaya, M. Bechelany, S. Balme and P. Miele, J. Mater. Chem. A **2**, 20650 (2014). https://doi.org/10.1039/C4TA05239K

27. C. Pacholski, A. Kornowski and H. Weller, Angew. Chem. Int. Ed. **41**, 1188 (2002). https://doi.org/10.1002/1521-3773(20020402)41:7<1188::AID-ANIE1188>3.0.CO;2-5

28. J. F.Banfield, S. A Welch, H.Zhang, et al., Science **289**, 751 (2000). https://doi.org/10.1126/science.289.5480.751

29. R. L. Penn and J. F. Banfield, Science **281**, 969 (1998). https://doi.org/10.1126/science.281.5379.969

30. R. L. Penn and J. F. Banfield, Geochim. Cosmochim. Acta **63**, 1549 (1999). https://doi.org/10.1016/S0016-7037(99)00037-X

31. S. M.Lee, S. N. Cho and J. W. Cheon, Adv. Mater. **15**, 441 (2003). https://doi.org/10.1002/adma.200390102

32. S. Music, S. Popovic, M. Maljkovic, J. Alloys Compd. **347**, 324 (2002). https://doi.org/10.1016/S0925-8388(02)00792-2

33. F. Xian, W. Bai, L. Xu, Mater. Lett. **108**, 46 (2013). https://doi.org/10.1016/j.matlet.2013.06.100

34. E. D. Bøjesen, K. M. Ø. Jensen, C. Tyrsted, et al., Cryst. Growth Des. **14**, 2803 (2014). https://doi.org/10.1021/cg5000606

35. S. Hayashi, N. Nakamori, H. Kanamori, et al., Surface Sci. **86**, 665 (1979). https://doi.org/10.1016/0039-6028(79)90447-3

36. Z. Zhang, Y. Lv, J. Yan, et al., J. Alloys Compd. 650, 374 (2015). https://doi.org/10.1016/j.jallcom.2015.07.162

37. Yeo-Chang Yoon, Kyoung-Seok Park, and Sam-Dong Kim, Thin Solid Films **597**, 125 (2015). https://doi.org/10.1016/j.tsf.2015.11.040

38. M. Andres-Verges, A. Mifsud, C.J. Serna, J. Chem. Soc., Faraday Trans. **86**, 959(1990). https://doi.org/10.1039/FT9908600959

39. M.H. Huang, Y. Wu, H. Feick, M. Tran, E. Weber, and P. Yang, Adv. Mater. **13**, 113 (2001). https://doi.org/10.1002/1521-4095(200101)13:2<113::AID-ADMA113>3.0.CO;2-H

40. B.X. Lin and Z.X. Fu, Appl. Phys. Lett. **79**, 943 (2001). https://doi.org/10.1063/1.1394173

41. J. Zhang, L.D. Sun, J.L. Yin, et al., Chem. Mater. **14**, 4172 (2002). https://doi.org/10.1021/cm020077h

42. S. Irshad, A. Salamat, A. Ahmed, et al., Cogent Chem. **4**, 1469207 (2018). https://doi.org/10.1080/23312009.2018.1469207

43. B. Y. Geng, G. Z. Wang, Z. Jiang, et al., Appl. Phys. Lett. **82**, 4791 (2003). https://doi.org/10.1063/1.1588735

44. J.Q. Hu and Y. Bando, Appl. Phys. Lett. **82**, 1401 (2003). https://doi.org/10.1063/1.1558899

45. S. Monticone, R. Tufeu, and A.V. Kanaev, J. Phys. Chem. B **102**, 2854 (1998). https://doi.org/10.1021/jp973425p

46. Y.W. Wang, L.D. Zhang, G.Z. Wang, et al., J. Cryst. Growth **234**, 171(2002). https://doi.org/10.1016/S0022-0248(01)01661-X

47. L. Guo, Y.L. Ji, H. Xu, et al., J. Am. Chem. Soc. **124**, 14864 (2002). https://doi.org/10.1021/ja027947g

48. Y.C. Zhang, X. Wu and X.Y. Hu, J. Cryst. Growth **280**, 250 (2005). https://doi.org/10.1016/j.jcrysgro.2005.03.001

49. M. Castellano and E. Matijevic, Chem. Mater. **1**, 78 (1989). https://doi.org/10.1021/cm00001a018

50. I. Martinez, C. Sanchez-Valle, I. Daniel, et al., Chem. Geol. **207**, 47, (2004). https://doi.org/10.1016/j.chemgeo.2004.02.003

51. Q. Li, V. Kumar, Y. Li, H. Zhang, T. J. Marks, et al., Chem. Mater. **17**, 1001 (2005). https://doi.org/10.1021/cm048144q

52. L. Vayssieres, N. Beermann, S.E Lindquist, et al., Chem. Mater. **13**, 233 (2001). https://doi.org/10.1021/cm001202x

53. L. Vayssieres, Adv. Mater. **15**, 464 (2003). https://doi.org/10.1002/adma.200390108

54. D. Ivakin Yu, M. N. Danchevskaya and G. P. Muravieva, Russ. J. Phys. Chem. B **13**, 1189 (2019). https://doi.org/10.1134/S199079311907011X

55. V. Gerbreders, M. Krasovska, E. Sledevskis, et al., Cryst. Eng. Comm. **22**, 1346 (2020). https://doi.org/10.1039/C9CE01556F